Fast evaluation of the current driven by electron cyclotron waves for reactor studies

E. Poli[1,*], M. Müller[1], H. Zohm[1], M. Kovari[2]

[1] *Max-Planck-Institut für Plasmaphysik, Garching bei München, Germany*
[2] *CCFE, Culham Science Centre, Abingdon, UK*

[*] Corresponding author: emanuele.poli@ipp.mpg.de

Abstract: Injection of electromagnetic waves in the electron-cyclotron (EC) frequency range is one of the most promising schemes to drive part of the plasma current in a tokamak fusion reactor. The theoretical calculation of the driven current, as usually performed by ray/beam tracing codes, relies on the knowledge of the magnetic equilibrium, the electron density and temperature profiles on the one hand and of the wave injection parameters on the other. If the *optimum* current drive efficiency for a given scenario is sought, extensive parameter scans are usually performed to determine the best injection conditions. This is however not a viable approach in typical systems-code applications, where the plasma configuration is not provided in sufficient detail and parameter scans would be anyway too demanding from the computational point of view. In this case, a different approach is required. In this paper, a procedure for the evaluation of the optimum current driven by EC waves for given global parameters is proposed, which relies on a single numerical calculation of the current drive efficiency, based on the adjoint method (including momentum-conserving corrections). The results are shown to be in good agreement with the full numerical optimization of the EC current drive efficiency for a variety of reactor relevant scenarios. This simplified approach also helps clarify the physics underlying the optimum current-drive conditions and the limitations to the achievable current-drive efficiency in reactor-grade plasmas.

Keywords: Plasma physics, magnetic confinement, wave-plasma interactions, electron cyclotron waves, current drive.

1 Introduction

A current produced by the injection of electromagnetic waves in the electron cyclotron (EC) frequency range will likely be essential in tokamak fusion reactors as an actuator for the control of magnetohydrodynamic instabilities (sawteeth and neoclassical tearing modes in particular, see e.g. [1]) and is a strong candidate to support steady state operation [2], considering that the EC current-drive (CD) efficiency can reach values close to those of neutral-beam current drive, at least on-axis, and that the wall-plug efficiency might be higher [3].

The impact of a current driven by auxiliary heating systems on the overall performance of a reactor can be evaluated employing reactor systems codes like `PROCESS` [4, 5]. Such codes aim to assess the engineering and economic viability of a hypothetical fusion power station using simple models of all parts of the reactor system. One element of the physical model is thus the calculation of the ECCD efficiency. This implies some essential differences with respect to the way ECCD calculations are mostly performed. The determination of EC driven current is usually achieved through tracing the path of one or more EC beams through the plasma using a ray or beam tracing code and evaluating the current drive efficiency along the beam path [6]. This requires the knowledge of the corresponding tokamak configuration (magnetic equilibrium, electron temperature and density profiles,

effective charge) and launch parameters (antenna position, wave frequency, injection angles). The maximum current achievable through the EC waves for a given plasma scenario can be determined in this case e.g. by scanning the five-dimensional parameter space given by the poloidal and toroidal injection angles, the wave frequency $\omega/2\pi$ and antenna coordinates (R, Z), as described in [3]. This strategy is not suitable for the exploration of the ECCD parameter space of a possible fusion reactor, as required for systems codes, for two basic reasons. First of all, scanning the injection angles in the relevant range with sufficient resolution for a reasonable set of frequencies and antenna positions would be too time-consuming, even if a single beam trace, entailing the calculation of the corresponding current-drive profile, can be performed on a time scale below one second [7]. This approach would be prohibitive for a systems code, in which the evaluation of the ECCD efficiency is just a small step in a much more extended optimization loop. The second reason is that in scoping studies several standard input elements for ray/beam tracing codes are not available. In particular, a consistent magnetic equilibrium is usually not computed and the profiles are known only through suitable analytic parameterizations.

The goal of the present paper is to describe a way to obtain a reliable estimate of the maximum ECCD efficiency achievable for given global tokamak parameters, to be included within the optimization procedure implemented in systems codes. A new module, called `HARE` (for: Hare Analyzes Reactor Eccd), has been developed and tested against full ECCD optimizations performed for existing reactor-relevant scenarios with the code `TORBEAM` [8, 7]. The calculation of the ECCD efficiency itself is based on the so-called adjoint method [9]. This involves basically the numerical evaluation of two one-dimensional integrals, in which he integrand itself might be known in integral form (see the brief overview in Sec. 2 below). This approach is, therefore, already very efficient numerically. Further ways to make it even faster with a limited loss of physics accuracy are known, as discussed later. The emphasis of this study is rather on the procedure followed to determine the parameters (in particular those related to the wave beam, like the frequency and the injection angle relative to the magnetic field) needed to calculate the maximum total current through the computation of the current drive efficiency for a single representative point in parameter space.

The paper is structured as follows. Sec. 2 is devoted to a summary of the theoretical background needed to follow the derivations presented later. Sec. 3 discusses the strategy usually employed to determine the optimum ECCD efficiency when a given scenario is available (in terms of magnetic configuration and kinetic profiles) and highlights some common features of different optimum-ECCD scenarios. The various steps leading to the development of the `HARE` module are detailed in Sec. 4, which also presents a comparison between the results of `HARE` and those from full `TORBEAM` optimization for a number of possible reactor scenarios. Discussion and conclusions follow in Sec. 5.

2 Theoretical background

In order to keep the paper self-contained, a brief overview of the basic theoretical results which underlie the calculation of the ECCD efficiency as performed routinely by ray/beam tracing codes is presented. Only the elements needed to follow the developments of our new approach presented later in this paper are discussed.

2.1 Adjoint method

A quantitative prediction of the current drive efficiency is based on the solution of the steady-state quasilinear kinetic equation for the distribution function f in the presence of collisions and heating. The basic ideas can be understood without involving the details related to the toroidal geometry. The relevant equation takes the symbolic form

$$C(f) + Q(f) = 0, \tag{1}$$

which represents the balance between the heating term Q, which acts to increase the energy of the particles (forcing the particles in the direction $\hat{\mathbf{v}} \equiv \mathbf{v}/v$ in velocity space) and the collision operator C, which forces the distribution function towards isotropization and thermalization. The heating operator can be written as the velocity-space divergence of the phase-space flux $\mathbf{S}_{\mathrm{rf}}$ induced by the radio-frequency waves [10] and the previous equation becomes

$$-C(f_1) = -\frac{\partial}{\partial \mathbf{v}} \cdot \mathbf{S}_{\mathrm{rf}}(f_M) \tag{2}$$

where f_1 is the perturbed electron distribution function, which is needed for the calculation of the current density

$$j = -e \int v_{\parallel} f_1 \mathrm{d}^3 v \tag{3}$$

(the symbols $\parallel$ and $\perp$ refer to the projections along and perpendicular to the direction of the confinement magnetic field, respectively).In the quasi-linear approximation, $Q = Q(f_M)$ holds, where f_M is the Maxwell distribution function. Given the form of Eq. (3), it is convenient to look for the solution of an auxiliary equation for the so-called response function χ

$$-C^{\dagger}(\chi) = v_{\parallel}, \tag{4}$$

where the adjoint operator $C^{\dagger}$ satisfies

$$\int f_1 C^{\dagger}(\chi) \mathrm{d}^3 v = \int \chi C(f_1) \mathrm{d}^3 v. \tag{5}$$

Substituting Eq. (4) for $v_{\parallel}$ into Eq. (3) and using Eq. (5) one has

$$j = e \int \chi C(f_1) \mathrm{d}^3 v \tag{6}$$

Upon inserting Eq. (2) and integrating by parts (assuming as usual vanishing boundaries at infinity), one can relate the current to the wave-induced flux $\mathbf{S}_{\mathrm{rf}}$ and the response function χ:

$$j = -e \int \mathbf{S}_{\mathrm{rf}} \cdot \frac{\partial \chi}{\partial \mathbf{v}} \mathrm{d}^3 v. \tag{7}$$

The main task is thus to find the response function χ as a solution of Eq. (4). This is usually done considering the so-called high-speed limit of the collision operator and gives the result [11]

$$\chi = \frac{v_{\parallel}}{(5 + Z_{\mathrm{eff}})\nu_e} \frac{v^3}{v_{\mathrm{th},e}^3} = \frac{v_{\parallel}}{(5 + Z_{\mathrm{eff}})\nu(v)}, \tag{8}$$

where Z_{eff} is the effective charge. The last step makes explicit use of the asymptotic scaling of the electron-electron collision frequency $\nu(v) = \nu_e v_{\mathrm{th},e}^3 / v^3$, where $v_{\mathrm{th},e}$ is the electron thermal speed and $\nu_e = e^4 n_e \ln\Lambda / 2\pi\epsilon_0^2 m^2 v_{\mathrm{th},e}^3$ (with the elementary charge e, the electron density n_e, the Coulomb logarithm $\ln\Lambda$ and the electron rest mass m).The absorbed power density is by definition

$$p = \int \frac{mv^2}{2} Q \mathrm{d}^3 v = -\int \frac{mv^2}{2} \frac{\partial}{\partial \mathbf{v}} \cdot \mathbf{S}_{\mathrm{rf}} \mathrm{d}^3 v = \int \frac{m}{2} \mathbf{S}_{\mathrm{rf}} \cdot \frac{\partial v^2}{\partial \mathbf{v}} \mathrm{d}^3 v \tag{9}$$

(last step after integration by parts). For a cyclotron resonance one can write $\mathbf{S}_{\mathrm{rf}} = S(f_M)\delta_{\mathrm{res}}\hat{\mathbf{v}}_{\perp}$, where δ_{res} denotes symbolically the resonance condition discussed in Sec. 2.2. The current drive efficiency is thus

$$\eta \equiv \frac{j}{p} = -\frac{e}{m} \frac{\int S(f_M)\delta_{\mathrm{res}} \partial\chi/\partial v_{\perp} \mathrm{d}v_{\parallel} v_{\perp} \mathrm{d}v_{\perp}}{\int S(f_M)\delta_{\mathrm{res}} v_{\perp} \mathrm{d}v_{\parallel} v_{\perp} \mathrm{d}v_{\perp}}. \tag{10}$$

In the integrals above, the variables $v_\parallel$ and $v_\perp$ are not independent, since the integration has to be performed on the curve in velocity space on which the resonance condition is satisfied. This reduces them actually to one-dimensional integrals. With χ given by Eq. (8), and replacing the resonance curve with a single point for the sake of simplicity, one has

$$\eta = -\frac{3e}{(5+Z_{\rm eff})m}\frac{v_\parallel v}{\nu_e v_{{\rm th},e}^3} \tag{11}$$

Since ν_e is proportional to the electron density n_e, Eq. (11) yields the approximate dependence $\eta \propto v^2/n_e$ (with $v_\parallel \simeq v$). Assuming that the energy of the resonant electrons scales with the electron temperature T_e (an assumption which will be discussed in Sec. 4.4), one gets the basic scaling

$$\eta \propto \frac{T_e}{n_e} \tag{12}$$

which is widely used for the interpretation of experimental results and extrapolation to reactors.

Eq. (8) was derived ignoring effects related to special relativity and toroidal geometry. If these are included, the determination of the response function χ becomes more involved, but the basic physics picture remains the same. The function χ can be written as the product of a part dependent on the magnitude of the normalized momentum $u = |\mathbf{u}| = \gamma v/c$ (γ being the Lorentz factor) and a part which depends on the pitch-angle variable $\lambda = (B_{max}/B)(u_\perp^2/u^2)$, where B_{max} is the maximum of the magnetic field B on a given flux surface. Following the notation of Ref. [12], this can be written as

$$\chi = F(u)H(\lambda). \tag{13}$$

Interestingly, the most complete model available to date for $F(u)$, which includes momentum conservation in electron-electron collisions [13, 14], is based on a simple (fourth-order polynomial) formula and thus lends itself to straightforward evaluation. This is the model used in all the `TORBEAM` calculations presented in this paper as well as in the `HARE` module.

The pitch-angle part of the response function $H(\lambda)$ is given by

$$H(\lambda) = \frac{\Theta(1-\lambda)}{2}\int_\lambda^1 \frac{{\rm d}\lambda'}{\langle(1-\lambda' B/B_{max})^{1/2}\rangle} \tag{14}$$

(angular brackets denote flux-surface average and Θ is the Heaviside function). A useful interpolation formula for the integrand is available [12], so that the evaluation of H reduces to the computation of a 1D integral. The velocity-space integrals defining η contain hence a function which is defined itself through an integral. A simplified expression for H can be obtained in the frame of the so-called square-well model employed by Cohen [15], according to which this function can be expressed in terms of Legendre functions. Even more drastically, one could neglect the effect of trapped particles altogether.

The expression $S(f_M)$ appearing in the expression of j and p contains in general Bessel functions, which however can be Taylor-expanded exploiting the fact that the electron gyroradius is in the applications usually much smaller than the wavelength of the EC beam. Further simplifications of the quasi-linear diffusion coefficient (e.g. considering only one wave-field polarization) are in principle possible.

2.2 The resonance condition

Along the beam path, the energy carried by the wave is transferred to the electrons in the plasma satisfying the relativistic resonance condition [16]

$$\omega - \frac{n\Omega}{\gamma} - k_\parallel v_\parallel = 0, \tag{15}$$

where ω is the frequency of the injected wave, n is the harmonic number and $k_\parallel$ is the component of the wave vector parallel to the magnetic field (satisfying the local dispersion relation). The last term represents the Doppler shift of the resonance with respect to the electron cyclotron frequency $\Omega = eB/m$ which is a function of position through the magnetic field B. Introducing $N_\parallel = ck_\parallel/\omega$, referred to as the parallel refractive index, and $\overline{\Omega} = \Omega/\omega$, the resonance condition can also be written as

$$\gamma - N_\parallel u_\parallel - n\overline{\Omega} = 0. \tag{16}$$

Using $\gamma = \sqrt{1 + u_\parallel^2 + u_\perp^2}$ one finds that the resonance curve in momentum space is represented by a half-ellipse (only values $u_\perp > 0$ are considered):

$$(1 - N_\parallel^2)\left(u_\parallel - \frac{N_\parallel}{1 - N_\parallel^2} n\overline{\Omega}\right)^2 + u_\perp^2 = \frac{n^2\overline{\Omega}^2}{1 - N_\parallel^2} - 1. \tag{17}$$

The intersection with the $u_\parallel$-axis is found for

$$u_{\parallel\mp} = \frac{nN_\parallel\overline{\Omega} \mp \sqrt{n^2\overline{\Omega}^2 - (1 - N_\parallel^2)}}{1 - N_\parallel^2}. \tag{18}$$

For each harmonic, resonance is possible only if

$$n\overline{\Omega} > \sqrt{1 - N_\parallel^2}. \tag{19}$$

For low-field side injection, this defines the first point in resonance (the so-called pinch point)

$$u_{\parallel pp} = \frac{nN_\parallel\overline{\Omega}}{1 - N_\parallel^2} = \frac{N_\parallel}{\sqrt{1 - N_\parallel^2}} \tag{20}$$

which can be seen as a degenerate case of the ellipse given by Eq. (17).

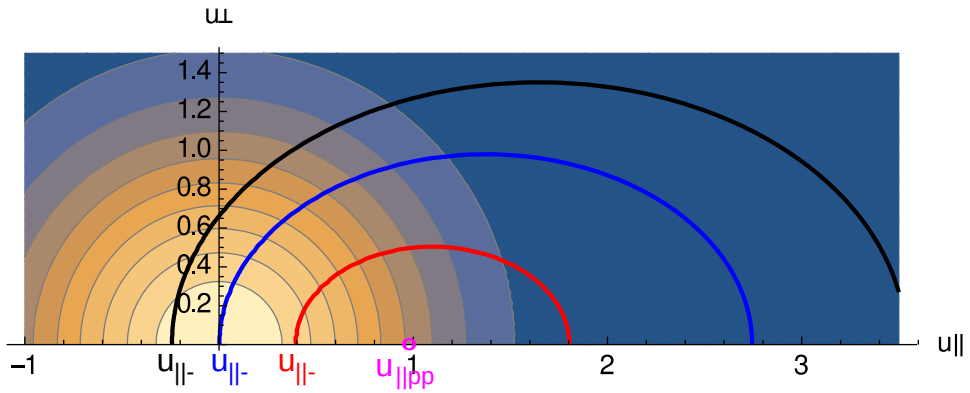

Figure 1: *Relativistic resonance curves for $N_\parallel = 0.7$, harmonic number $n = 1$ and different values of $\overline{\Omega}$ (red: $\overline{\Omega} = 0.8$; blue: $\overline{\Omega} = 1$; black: $\overline{\Omega} = 1.2$). The intersection $u_{\parallel-}$ of the resonance curves with the $u_\parallel$-axis is also shown, together with the pinch-point position $u_{\parallel pp} \simeq 0.98$, magenta circle. Maxwellian isocontours centred at $(u_\parallel, u_\perp) = (0, 0)$ are also shown.*

Fig. 1 shows the resonance ellipses for three different values of $\overline{\Omega}$. Note that $u_{\parallel-} = 0$ for $n\overline{\Omega} = 1$. In usual high-ECCD scenarios relying on the Fisch-Boozer effect [17], the power carried by the wave is absorbed before $u_{\parallel-}$ crosses the origin. The strongest wave-particle interaction occurs around $u_{\parallel-}$, since this is the point on the resonance curve closest to the

Maxwellian bulk, where most electrons are available (in situations with $N_\parallel < 0$, the role of $u_{\parallel -}$ and $u_{\parallel +}$ is reversed).

The determination of the optimum current drive conditions is intimately related to finding a compromise between high CD efficiency, which favours high-energy (low-collisionality) electrons, and complete absorption within (a reasonably narrow region of) the plasma, which requires a sufficient number of resonant electrons and hence favours the region of velocity space close to the thermal bulk. This is the basic point of the analysis presented in Sec. 4.

3 ECCD optimization for a specific reactor scenario

If a tokamak scenario is available in terms of magnetic equilibrium and kinetic profiles, the maximum amount of current which can be driven through EC waves can be determined by exploring the parameter space defined by the injection angles, the wave frequency $\omega/2\pi$ and the antenna position (R, Z) in the poloidal plane.For the magnetic field strength usually considered for a reactor, the envisaged heating scheme is O-mode at the fundamental ($n = 1$) harmonic. In reactor-grade plasmas, where the core temperature is in the range $T_e \gtrsim 30$ keV (the Boltzmann constant is set to one in this paper for simplicity and the temperature is treated as an energy), the beam can be prone to parasitic absorption from the second harmonic, which reduces the power available for current drive at the fundamental harmonic. In this respect, an elevated antenna position turns out to be more favourable than an outboard-midplane injection, since it allows the "major-radius" coordinate R of the antenna to be reduced, thus shortening the path between the launcher and the $n = 1$ resonance [3].

In this work, we considered a set of reactor-relevant scenarios, corresponding to different EU-DEMO design options.

	R_0 [cm]	a [cm]	B_0 [T]	n_{e0} [10^{19} m^{-3}]	T_{e0} [keV]	Z_{eff}
ITER	620	201	5.3	10.56	24.49	1.76
DEMO1	907	292	5.66	10.50	33.25	2.0
DEMO2 nflat	749.9	288.5	5.627	9.94	31.17	4.18
DEMO2 npeak	749.9	288.5	5.627	17.99	23.50	4.13
flexi-DEMO	840	270	5.8	10.6	41.19	1.13

Table 1: *Global parameters for the investigated scenarios.*

The fundamental parameters of these scenarios (respectively, the major radius R_0, the minor radius a, the nominal magnetic field B_0, the central electron densities and temperatures n_{e0} and T_{e0} and the effective charge) are summarized in Table 1. In addition, a half-temperature DEMO1 scenario (where all parameters are taken as in the DEMO1-case, but the temperature is divided by two) has been added in order to enlarge the dataset to lower temperatures.

The typical result of an ECCD scan over a range of launch angles using `TORBEAM` for given frequency and antenna position is shown in Fig. 2 for DEMO1 parameters. In this case, the maximum current drive is found for a poloidal injection angle $\alpha = 46°$ and a toroidal injection angle $\beta = 38°$.The calculation retains the contribution to the current drive efficiency of each harmonic separately, as described in [7]. The absorption is calculated using the routine originally developed for the `GRAY` code [18, 19]. It can be seen that the maximum current drive is practically on axis ($\rho < 0.1$, where ρ is a normalized radial coordinate varying between 0 on the magnetic axis and 1 at the last closed flux surface).The radial extent of the region where significant absorption takes place, highlighted in black in the right panel of Fig. 2, is fairly large. This is a consequence of the non-negligible second-harmonic absorption in the region $0.2 \lesssim \rho \lesssim 0.6$ and of the fact that

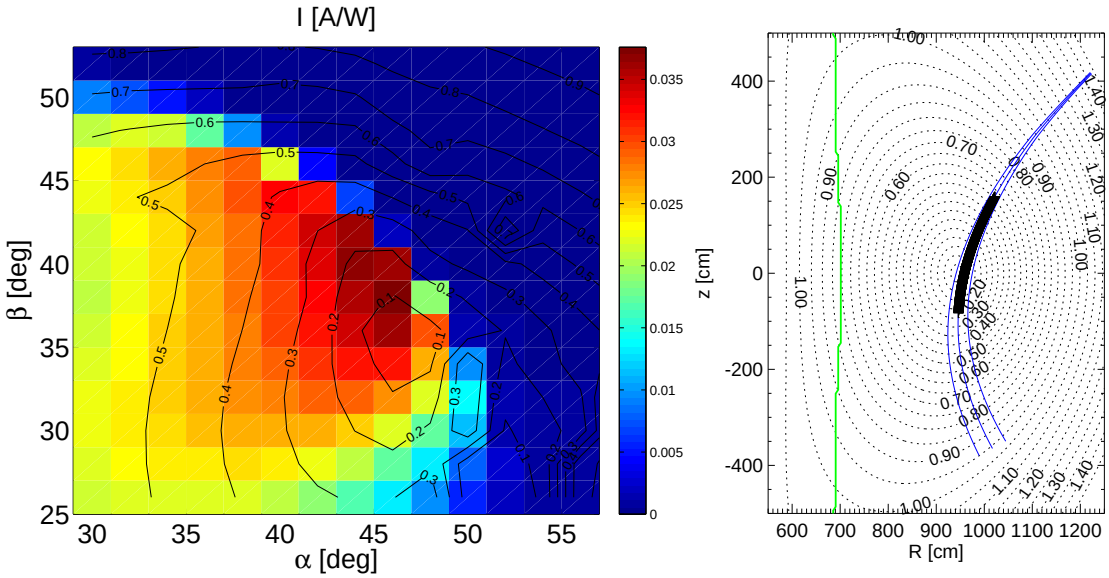

Figure 2: *Left: Driven current per unit of absorbed power (colour scale) with overlaid contours of the radial position ρ of maximum absorption (black contour lines) as a function of the poloidal and toroidal injection angles (α and β, respectively) for injection from $(R, Z) = (12.23, 4.17)$ m and wave frequency $\omega/2\pi = 225$ GHz and DEMO1 parameters. Right: Poloidal projection of the beam path for the $(\alpha, \beta) = (46°, 38°)$, corresponding to the maximum current drive shown in the left plot. The region where non-negligible absorption takes place is highlighted through the black thicker line along the central ray and is obtained by selecting the points for which the power* $\mathrm{d}P$ *absorbed in an integration step exceeds* 10^{-4} *times the injected power.*

the absorption at the $n = 1$ harmonic is not very strong, since the resonance condition is satisfied by electrons on the tail of the distribution function. Being more energetic, these electrons are less collisional and yield hence a higher current drive efficiency, as discussed above.

It is instructive to have a closer look at the quantities which determine the current drive efficiency according to the discussion in Sec. 2. In Fig. 3 (left), the values of $u_{\parallel -}$ and $N_\parallel$ (left) along the central ray for the beam path shown in Fig. 2 are reported. While the parallel refractive index remains nearly constant, the minimum intercept $u_{\parallel -}$ of the resonance condition with the $u_\parallel$-axis, cf. Sec. 2.2, is negative where the absorption takes place on the second harmonic only, while it jumps to large positive values as soon as the pinch point for $n = 1$, given by Eq. (20), is reached around $\rho = 0.22$. Correspondingly, the energy $\mathcal{E} = mc^2(\gamma - 1)$ (with c the speed of light) of the resonant electrons calculated for $u_\perp = 0$ and $u_\parallel = u_{\parallel -}$, reported in the right panel, jumps first to high values (eight times T_e) and then quickly decreases until it attains a value $\mathcal{E} \simeq 4T_e$ at the point of strongest absorption (denoted by a black cross). This is defined as the point corresponding to the largest value of the absorbed power $\mathrm{d}P$ in a single integration step along the central ray. Following the power delivered to the plasma in the right panel, it can be seen that less than 10% of the power is absorbed in the region of second-harmonic interaction. Soon after the first harmonic becomes accessible, the absorption becomes much stronger until eventually the whole power is transferred to the plasma.

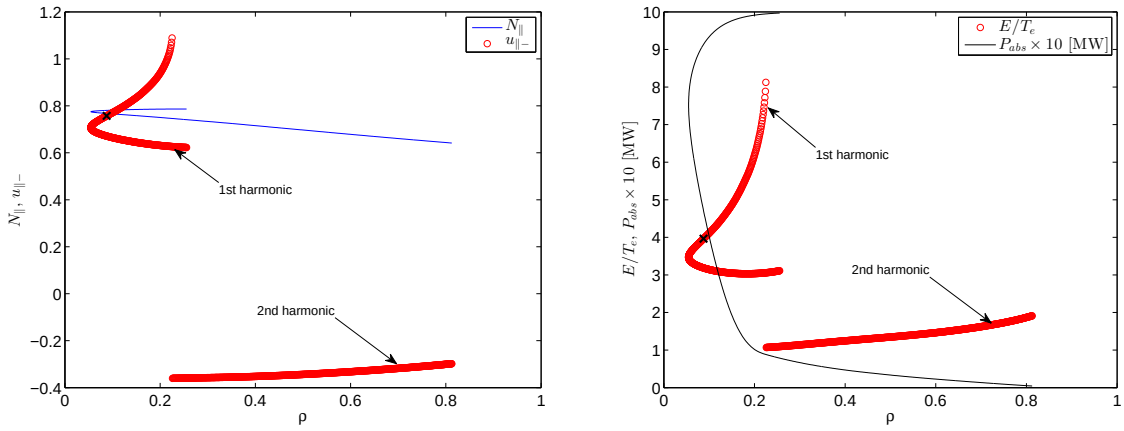

Figure 3: *The values of $u_{\parallel -}$, $N_\parallel$ (left) and $mc^2(\sqrt{u_{\parallel -}^2 + 1} - 1)/T_e$ and power absorbed by the plasma P_{abs} as a function of the normalized minor radius ρ for the optimum-ECCD case shown in Fig. 2. The black cross shows the point of maximum absorption.*

4 Evaluation of ECCD from global tokamak parameters

As already stated above, the calculation of the ECCD efficiency based on the adjoint method is computationally straightforward. Possible ways to speed up this step have been discussed shortly at the end of Sec. 2.1. The goal of this section is to present a reliable procedure for the evaluation of the total current which can be driven by EC waves for given global tokamak parameters, based on a single numerical evaluation of the CD efficiency η. This is assumed to be an affordable computational endeavour in the frame of systems code applications.

The quantities required for the numerical determination of the CD efficiency at a given point in the plasma are the parallel and perpendicular components of the wave refractive index, the components of the unit wave electric field, the electron temperature, the ratios ω_p^2/ω^2 and Ω^2/ω^2 (ω_p being the electron plasma frequency) at a given location, the minimum and maximum magnetic field on the corresponding flux surface, the poloidal angle θ at which the absorption takes place, the vacuum wavevector $k_0 = \omega/c$ and the effective charge. Some of the plasma parameters needed to compute these input values, like density, temperature, magnetic field and effective charge at the position of interest can be assumed to be known (in systems codes, density and temperature profiles are usually parametrized as analytic functions of ρ [4]. Extensions to include profiles originating from physics-based transport and equilibrium modelling are under way [20, 21]). The same is true for the minimum and maximum magnetic field on a given flux surface. The poloidal angle at which the beam crosses the flux surface can also be inferred (optimum current drive is usually achieved for injection from an elevated position, as discussed in the previous section). In the following, we will set this angle to 60°. It has been verified that this parameter does not influence the current drive efficiency significantly, its variation being below 4.1% for a variation of θ by $\mp 10°$ for the results presented in Sec. 4.5.

The challenging point is the selection of the injection angle (hence $N_\parallel$) and the wave frequency (once ω and $N_\parallel$ have been fixed, the dispersion relation determines $N_\perp$ and the wave polarization). The fundamental relation between ω and $N_\parallel$ is given by the resonance condition (15), which further involves the particle energy through the Lorentz factor γ. As discussed in Sec. 2, the condition of optimum current drive corresponds to resonant (current-carrying) electrons with the highest possible energy which still ensures sufficient absorption. In Sec. 4.1, a constraint on the energy of the resonant electrons $\mathcal{E}/T_e$ is

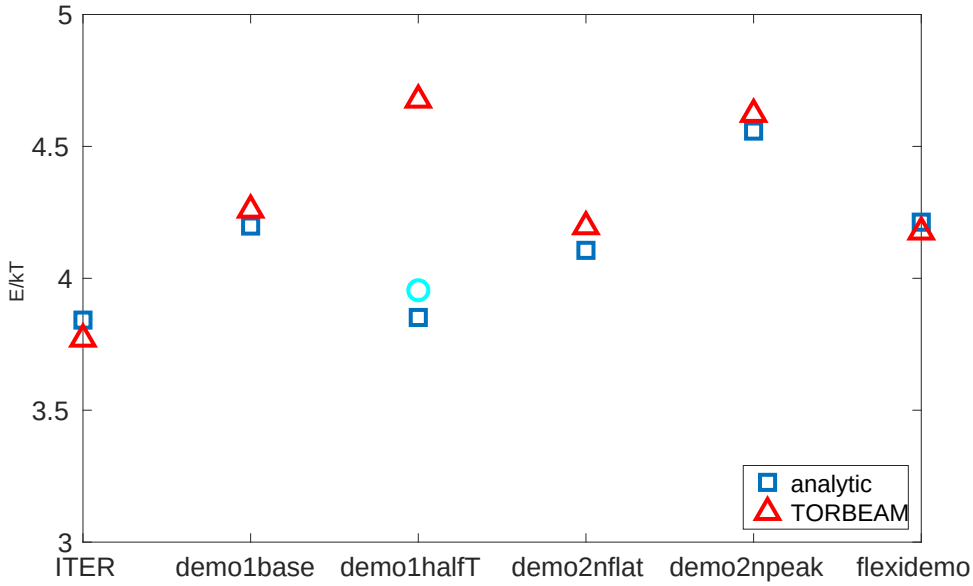

Figure 4: *Value of the energy of resonant electrons (normalized to the electron temperature) as obtained from Eq. (24) for different machine parameters (blue squares). The red triangles show the corresponding values from ECCD optimization for the same scenarios. The cyan circle for the DEMO1 half-temperature case shows the ratio $\mathcal{E}/T_e$ for a nearly-optimum case (for which the total driven current is ca. 4% lower than for the optimum case).*

derived. We assume that the interaction between wave and particles is strongest around the lower edge of the resonant range defined by Eq. (18), i.e. around $u_{\parallel -}$ (see discussion in Sec. 2.2), which allows us to set $u_\perp \simeq 0$. Then, the condition $\mathcal{E}/T_e = f_T$ fixes also $u_{\parallel -}$ through $\mathcal{E} \simeq mc^2(\sqrt{u_{\parallel -}^2 + 1} - 1)$, so that the resonance condition effectively defines a relation between $N_\parallel$ and ω. In order to determine both quantities separately, a further constraint is needed, as discussed in Sec. 4.2 and 4.3.

4.1 Energy of resonant electrons

In order to derive a (temperature-dependent) constraint for the energy of the resonant electrons at maximum current drive, we adapt the approach of Smith *et al.* [22] and require that the EC power is completely absorbed within a fraction f_{abs} of the minor radius a. Defining an "absorption length" as the inverse of the absorption coefficient α, this condition reads

$$\frac{1}{\alpha} = f_{abs} a. \tag{21}$$

A formula for the absorption coefficient of ordinary waves satisfying the $n = 1$ resonance for oblique propagation can be found in [23] and reads

$$\alpha_1^{(O)} = 2\sqrt{2}\frac{\omega_p^2}{\Omega^2}\frac{g^{(O)}}{4\pi}\sqrt{\frac{T_e}{mc^2}}\frac{\Omega}{c}\mathrm{Im}\left[-\frac{1}{Z(\zeta_1)}\right], \tag{22}$$

where Z is the plasma dispersion function of argument

$$\zeta_1 = \frac{\omega - \Omega}{\sqrt{2}k_\parallel v_{\mathrm{th},e}} = \frac{v_\parallel}{\sqrt{2}v_{\mathrm{th},e}} \simeq \sqrt{\frac{\mathcal{E}}{T_e}}, \tag{23}$$

and the factor $R^{(O)}$ of [23] has been written as in [22] isolating the factor ω_p^2/Ω^2 and dividing by 4π in order to have $g^{(O)}$ (factor depending mainly on injection geometry) of

order unity. With this expressions, Eq. (21) can be cast in the form of a condition for $f_T = \mathcal{E}/T_e$, namely

$$f_T = \frac{\mathcal{E}}{T_e} = \ln\left[\frac{f_{abs}}{|Z|^2}\sqrt{\frac{2\pi T_e}{mc^2}}\frac{\nu_c a}{c}\frac{\omega_p^2}{\Omega^2}g^{(O)}\right], \tag{24}$$

where $\nu_c = \Omega/2\pi$. In TORBEAM optimizations it is often found that optimum ECCD profiles have a width of the order of $\Delta\rho \simeq 0.2$, see e.g. Fig. 3b, so we set $f_{abs} = 1/5$. A brief discussion about this choice should be added here. Although the dependence of f_T on f_{abs} is only logarithmic, this choice also influences the constraint on the width of the absorption profile introduced in Sec. 4.3 and it has thus a noticeable influence on the final results. The fact that optimum ECCD conditions are often found for $\Delta\rho \simeq 0.2$ has its physical explanation in the fact that larger profiles (which might be thought to be preferable because of the relation between weaker absorption and higher current drive discussed before) start feeling the change in temperature and hence in ECCD efficiency far from the optimum point (typically the centre of the plasma column). In our model, a variation of $\Delta\rho$ by ∓ 0.1 leads to a change of the current-drive efficiency in the range of ca. $\mp 15\%$, whereas the best matching of the full TORBEAM results, reported in Sec. 4.5, is achieved for the value $\Delta\rho = 0.2$ selected here. This choice of $\Delta\rho$ (or equivalently f_{abs}) is basically the main "tuning parameter" employed in this model and can be justified as discussed above.

Approximating $|Z|^2 \simeq g^{(O)} \simeq 1$, one finds values for f_T in the range between 3.8 and 4.2 for typical ITER [24] and DEMO parameters, see Fig. 4. These match closely the values of $\mathcal{E}/T_e$ at maximum absorption found in TORBEAM runs corresponding to maximum ECCD for each scenario.

4.2 Frequency shift

A first consequence of imposing a given ratio between the energy of the resonant electrons and thermal energy can be appreciated if we fix the value of $N_\parallel$ as well (taking e.g. as a reference the typical values of $N_\parallel$ found in the TORBEAM optimizations described in Sec. 3). With the previous approximations, from $\mathcal{E} = mc^2(\gamma - 1)$ one can derive

$$\gamma = \frac{f_T T_e}{mc^2} + 1 \tag{25}$$

and

$$u_{\parallel -} = \sqrt{\left(\frac{f_T T_e}{mc^2} + 1\right)^2 - 1}. \tag{26}$$

Calculating Ω with the nominal (on-axis) magnetic field, the resonance condition, Eq. (15), can be used to express the shift of the wave frequency ω needed to have on-axis resonance for a given value of $N_\parallel$ as a function of the electron temperature

$$\frac{\omega}{n\Omega} = \left[\frac{f_T T_e}{mc^2} + 1 - N_\parallel\sqrt{\left(\frac{f_T T_e}{mc^2} + 1\right)^2 - 1}\right]^{-1}. \tag{27}$$

Fig. 5 (left panel, dotted green curve) shows that for typical central temperatures envisaged for a fusion reactor (20–40 keV) and $N_\parallel = 0.75$ (as typically found in ECCD optimization for DEMO parameters, cf. Fig. 3), the wave frequency needed to satisfy the resonance condition exceeds by a factor around 1.4 the cold-resonance cyclotron frequency, in agreement with previous studies [25, 3].

Eq. (27) has a maximum value $\omega/n\Omega = 1/\sqrt{1 - N_\parallel^2}$, which corresponds to the accessibility condition of the n-th resonance (19), at a temperature $T_e = (mc^2/f_T)(1/\sqrt{1 - N_\parallel^2} -$

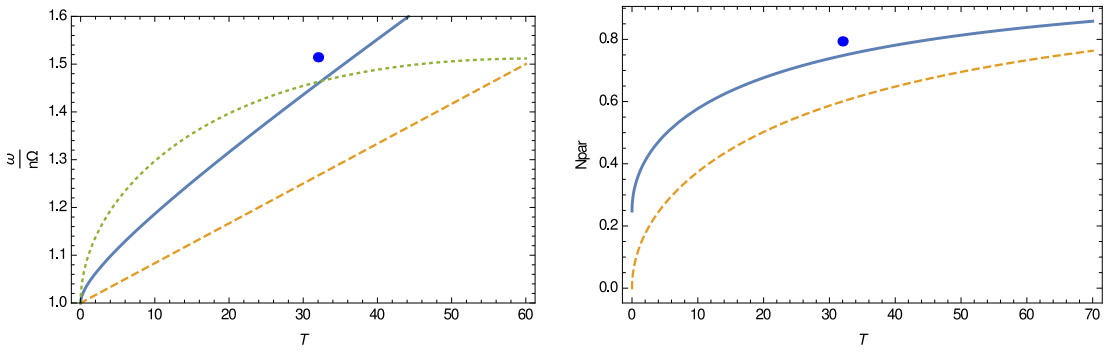

Figure 5: *Frequency shift (with respect to the cyclotron frequency on axis, left) and parallel refractive index $N_\parallel$ (right) as a function of the electron temperature. The yellow dashed lines are obtained by imposing $f_T = 4.26$ at the pinch point, Eq. (28) and Eq. (29) respectively, while the blue solid lines are obtained by imposing $f_T = 4.26$ at the position of maximum absorption and $\Delta R = R_{pp} - R_a = f_{abs} a \cos\theta$, see Eq. (33) and Eq. (32) below. The dotted green line in the left panel shows Eq. (27) with $N_\parallel = 0.75$ and $f_T = 4.26$. The blue points in both panels represent the value of $\omega/n\Omega$ resp. $N_\parallel$ found from* `TORBEAM` *ECCD optimization for DEMO1. The value f_T is also extracted from the* `TORBEAM` *optimization, cf. Fig. 4.*

1). This means that, for fixed $N_\parallel$, there is only one temperature for which the energy of the resonant electrons is $\mathcal{E} = f_T T_e$ at the pinch point.

On the other hand, one could note at this point that it is possible to select $N_\parallel$ such that the condition $\mathcal{E} = f_T T_e$ is always satisfied at the pinch point. Once $N_\parallel$ is determined in this way, the resonance condition determines the wave frequency ω. Equating $1/\sqrt{1 - N_\parallel^2}$ to the right-hand side of Eq. (27), one finds

$$N_\parallel = \sqrt{1 - \frac{1}{(f_T T_e/mc^2 + 1)^2}} \tag{28}$$

which leads to the simple expression for the frequency shift

$$\frac{\omega}{n\Omega} = \frac{f_T T_e}{mc^2} + 1. \tag{29}$$

Both $\omega/n\Omega$ and $N_\parallel$ as expressed by Eq. (29) and Eq. (28) exhibit a physically reasonable qualitative dependence on temperature, see the dashed yellow lines in Fig. 5. In particular, higher temperatures allow the resonance to shift to the tail of the distribution function still maintaining appreciable absorption and hence allow larger values of $N_\parallel$. Their values, however, are lower than those found in numerical optimizations (blue points in Fig. 5, where DEMO1 parameters have been taken as a reference). As a matter of fact, for typical cases of maximum ECCD, as shown for instance in Fig. 3, the condition $\mathcal{E} = f_T T_e$ as determined in Sec. 4.1 is not met at the pinch point (first point in resonance) but rather at the point of maximum absorption. At the pinch point, the energy of the resonant electrons is usually much higher, which ensures higher current drive efficiency, although at a relatively low absorption rate. In other words, imposing $\mathcal{E} = f_T T_e \approx 4T_e$ at the pinch point misses the contribution of the velocity-space region located in the range $4 \lesssim \mathcal{E}/T_e \lesssim 6$, which exhibits a high current-drive efficiency in conjunction with a non-negligible absorption.This suggests a different procedure for the determination of $N_\parallel$ and ω, introduced in the next section.

4.3 Constraint on the width of the absorption profile

We impose now the constraint $\mathcal{E} = f_T T_e$ at the position of maximum absorption. This is the "representative point" selected for the single evaluation of the ECCD efficiency

as envisaged in the method proposed here, i.e. the plasma parameters are evaluated at the point where the peak absorption (which is usually very close to the peak current drive) is required to be. The ECCD efficiency is typically higher on the low-field side of this point, i.e. moving towards the pinch point, while it is typically lower as the beam penetrates towards the high-field side and the resonance moves to less energetic electrons. The ECCD efficiency calculated at the point of maximum absorption can be thought to represents thus a sort of average value across the absorption profile. This approach is tested in the following.

Besides the resonance condition, a further constraint that allows the determination of ω and $N_\parallel$ separately is still needed. Such a constraint is imposed by selecting the distance between pinch point and position of maximum absorption such that it coincides with the "absorption length" defined as $f_{abs}a$, see Eq. (21). This represents an approximation, as the particle energy at pinch point is usually very high (in the range of 8–9 T_e for typical optimum conditions) and correspondingly the absorption is still quite weak. However, given the fast decrease of $\mathcal{E}/T_e$ from the pinch point inwards, this approximation is well justified. This is clearly illustrated in Fig. 3 (right panel), which reports also the steep rise of the power delivered to the plasma once the energy of the resonant electrons drops below $\mathcal{E}/T_e \lesssim 6$. The major radius of the pinch point, R_{pp}, can be found from the relation $n\Omega_{pp}/\omega = \sqrt{1-N_\parallel^2}$, where Ω_{pp} is the cyclotron frequency evaluated at $R = R_{pp}$, cf. Eq. (19), and reads

$$R_{pp} = \frac{n\Omega_a}{\omega\sqrt{1-N_\parallel^2}} R_a. \tag{30}$$

The subscript a denotes the position of peak absorption (e.g. the magnetic axis), where the constraint $\mathcal{E} = f_T T_e$ is enforced. Consistently with the numerical simulations and with the fact that the absorption is assumed to be relatively well localized, the variation of $N_\parallel$ between the positions R_a and R_{pp} is assumed to be negligible.

Imposing $\Delta R = R_{pp} - R_a = f_{abs} a \cos\theta$ one obtains

$$\frac{R_{pp}}{R_a} = 1 + \frac{f_{abs} a}{R_a}\cos\theta, \tag{31}$$

which fixes the value of R_{pp} for given f_{abs}, R_a and θ. The resonance condition can now be used to express $N_\parallel$ as a function of ω and $u_{\parallel -}$ (fixed through f_T):

$$N_\parallel = \frac{1}{u_{\parallel -}}\left(\sqrt{u_{\parallel -}^2 + 1} - \frac{n\Omega_a}{\omega}\right). \tag{32}$$

Inserting Eq. (32) into Eq. (30) then determines uniquely the wave frequency ω as

$$\frac{\omega}{n\Omega_a} = \sqrt{u_{\parallel -}^2 + 1} + \sqrt{u_{\parallel -}^2\left(1 - \frac{R_a^2}{R_{pp}^2}\right)}, \tag{33}$$

where now all the quantities on the right-hand side are known. $N_\parallel$ is then computed from Eq. (32). The dependence of $N_\parallel$ and ω on the electron temperature is obtained inserting Eq. (26) into the previous expressions. Recalling $\gamma = f_T T_e/mc^2 + 1$, the previous equations lead to a nearly linear dependence of the frequency shift with T_e, while $N_\parallel$ scales approximately with the square root of T_e. The previous expressions are evaluated explicitly in Fig. 5 (solid blue lines). These values are much closer to the results found in numerical ECCD optimizations than those obtained in the previous section, where the condition on the energy of the resonant electrons was imposed at the pinch point. The `HARE` module implements Eqs. (32-33) as part of the procedure needed for the determination of the ECCD efficiency.

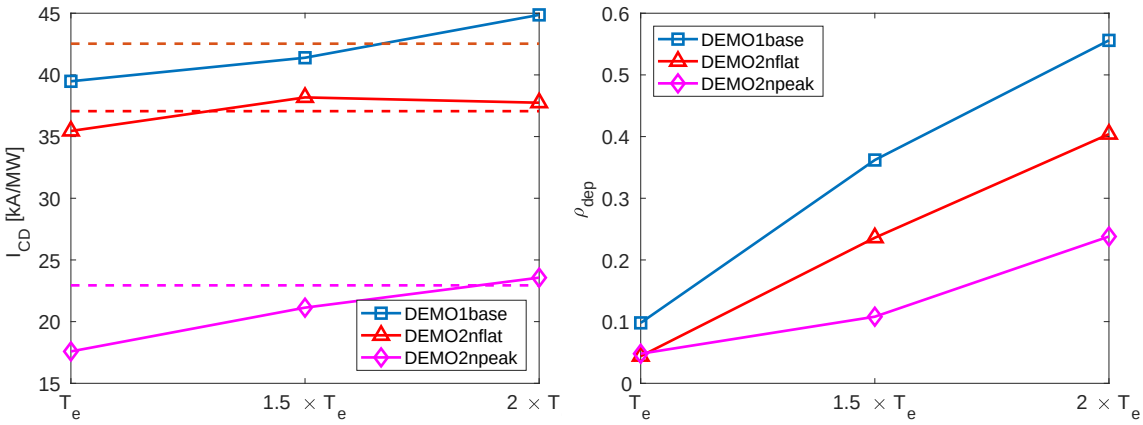

Figure 6: *Maximum driven current (left) and corresponding normalized deposition radius (right), for the three scenarios reported in the legend, as obtained from* `TORBEAM` *optimization. The temperature profile in the respective scenarios is rescaled by the factor indicated on the x-axis.*

4.4 Saturation of the ECCD efficiency for $T_e > 30$ keV

The equations derived in Sec. 4.3 suggest that a reactor could take advantage from higher and higher temperatures to push the resonance towards more and more energetic electrons and increase the CD efficiency indefinitely. Indeed, as discussed in Sec. 2.1, the "standard" scaling $\eta \propto T_e/n_e$ relies on the assumption that the energy of the resonant electrons available for current drive can be increased proportionally to T_e.

It has been shown by Smith *et al.* [22], however, that the current drive efficiency cannot be increased above a given limit, dictated by the condition that the absorption at the desired harmonic (in our case $n = 1$) exceeds the absorption due to the next harmonic. The influence of the next harmonic, called harmonic overlap, can be understood intuitively from the fact that increasing the wave frequency proportionally to the electron temperature, as suggested by Eq. (33), leads to a shift of the lower harmonic away from the plasma centre towards the high-field side, while the next harmonic is moved closer to the centre from the low-field side. Quantitatively, referring to Fig. 1 and the discussion in Sec. 2.2, it can be assumed that the next harmonic dominates the absorption process when the corresponding value of $|u_{\parallel -}|$ is lower (i.e. closer to the Maxwellian bulk) than the value of $|u_{\parallel -}|$ for the desired harmonic. For the $n = 1$-resonance, such a limit is found to occur [22] when the energy of the electrons resonating with the lower harmonic reaches a value of $mc^2(\sqrt{3/2}-1) \approx 115$ keV. Assuming that this energy corresponds to a multiple $f_T \approx 4$ of the electron temperature implies that there is no advantage in increasing the energy of the resonant electrons with the electron temperature if T_e exceeds a value around 30 keV. It should be noted that an implicit assumption in the analysis of Smith *et al.* is that the region around the pinch point contributes significantly to the absorption, while this turns out not to be strictly the case under ECCD-optimized conditions, cf. Fig. 3 and the discussion in Sec. 4.3, so that the T_e-threshold is somewhat higher. However, even for T_e just above 30 keV, the achievable current drive is often found to be limited by second-harmonic absorption *before* the pinch point. For this reason, in `HARE` the ECCD efficiency is calculated limiting the input temperature to 30 keV whenever the scenario exhibits a temperature above that value.

This approach has been tested by increasing the electron temperature for three selected scenarios (in each case by a factor 1.5 and 2) and optimizing the ECCD as outlined in Sec. 3. Whereas the DEMO1-baseline and the DEMO2-nflat scenarios have a nominal T_e slightly above 30 keV, for DEMO2-npeak the nominal electron temperature is 23.5 keV, so the ECDD efficiency is expected to be close to saturation in the first two cases and to reach saturation with increasing temperature in the last one. Fig. 6 confirms these expectations: the rise in I_{CD} is below 15% in the first two cases and about 35% in the last case; it is

recalled that according to the scaling $\eta \propto T_e/n_e$ the driven current should double across the range considered in Fig. 6 in all cases. These results show that capping the ECCD efficiency at temperatures above 30 keV leads to a good estimate of the saturation level. As it can be observed in the right panel, increasing the temperature shifts the position of the peak deposition under conditions of maximum current drive to larger radii. This is due to the fact that the region of plasma with $T_e > 30$ keV becomes larger and larger with increasing temperature, while a shorter path through the plasma reduces the second-harmonic absorption before the pinch point is reached. The issue of the radial distribution of the driven current is discussed in Sec. 4.6.

4.5 Comparison of the HARE model to ECCD optimization for selected scenarios

The approach described in Sections 4.3, 4.4 is now tested against results from scenario optimization to assess its reliability and accuracy. The input parameters for HARE are the ρ value at which the current should be estimated, the corresponding values of n_e, T_e and $Z_{\rm eff}$, the magnetic field on axis and the values of minor and major radius of the machine. All these quantities are available in the frame of systems-code applications. For central ECCD, the value of ρ is set to 0.1 to allow for the spread of ECCD profile. The total driven current is calculated as

$$I_{CD} = \frac{\eta P}{2\pi R_0}, \tag{34}$$

where the efficiency η is the output of the ECCD routine and P is the injected power. In this formula, the ratio between the flux-surface averages $\langle B_t/R\rangle/\langle B\rangle$ which should appear [12] as a prefactor on the right-hand side (B_t being the toroidal magnetic field), is approximated as $1/R_0$.

In Fig. 7, the values of the total driven current, optimum wave frequency, parallel refractive index, $u_{\parallel -}$ at maximum absorption and at pinch point returned by the HARE module are compared to those corresponding to the maximum current drive in TORBEAM scans. As explained in the previous section, the input electron temperature in HARE is set to 30 keV whenever the corresponding scenario exceeds this value. Although the parameters of the various scenarios (particularly density and temperature) differ significantly from each other, the HARE predictions are in good agreement with the reference values from TORBEAM optimizations in all cases. The largest differences can be observed for the value of $u_{\parallel -}$ at the pinch point. This is related to the fact that $u_{\parallel -}$ at the pinch point can vary significantly for relatively small changes of the radial extent of the region exhibiting first-harmonic absorption. As discussed above, the exact value of $u_{\parallel pp}$ does not influence significantly the total driven current.

Fig. 8 reports the percentage deviation of the HARE values from the reference values, calculated as $100 \times (I_{\rm HARE} - I_{\rm TORBEAM})/I_{\rm TORBEAM}$. The deviation is below 10% for all the scenarios explored.

It should be stressed that a scenario optimization is usually performed scanning 15×15 values of the poloidal and toroidal angles (cf. Fig. 2) for a number (usually $\gtrsim 10$) of launcher positions and frequencies, resulting in a few thousand TORBEAM runs, each requiring a couple of seconds. In contrast, the HARE module performs a single call to the ECCD routine, which has an execution time below 0.1 ms.

Simple scaling formulas for the ratio between the total EC current I_{CD} and the absorbed power P (for EC waves, this is usually assumed to coincide with the injected power), which would offer of course the advantage of a much faster execution time, have been found to be much less reliable than the model implemented in HARE. A figure of merit often employed in this respect is given by [26]

$$\zeta_{CD} = \frac{e^3}{\varepsilon_0^2}\frac{n_e R_0}{T_e}\frac{I_{CD}}{P} \approx 32.7\frac{n_{20} R_{\rm m} I_{\rm A}}{T_{\rm keV} P_{\rm W}}, \tag{35}$$

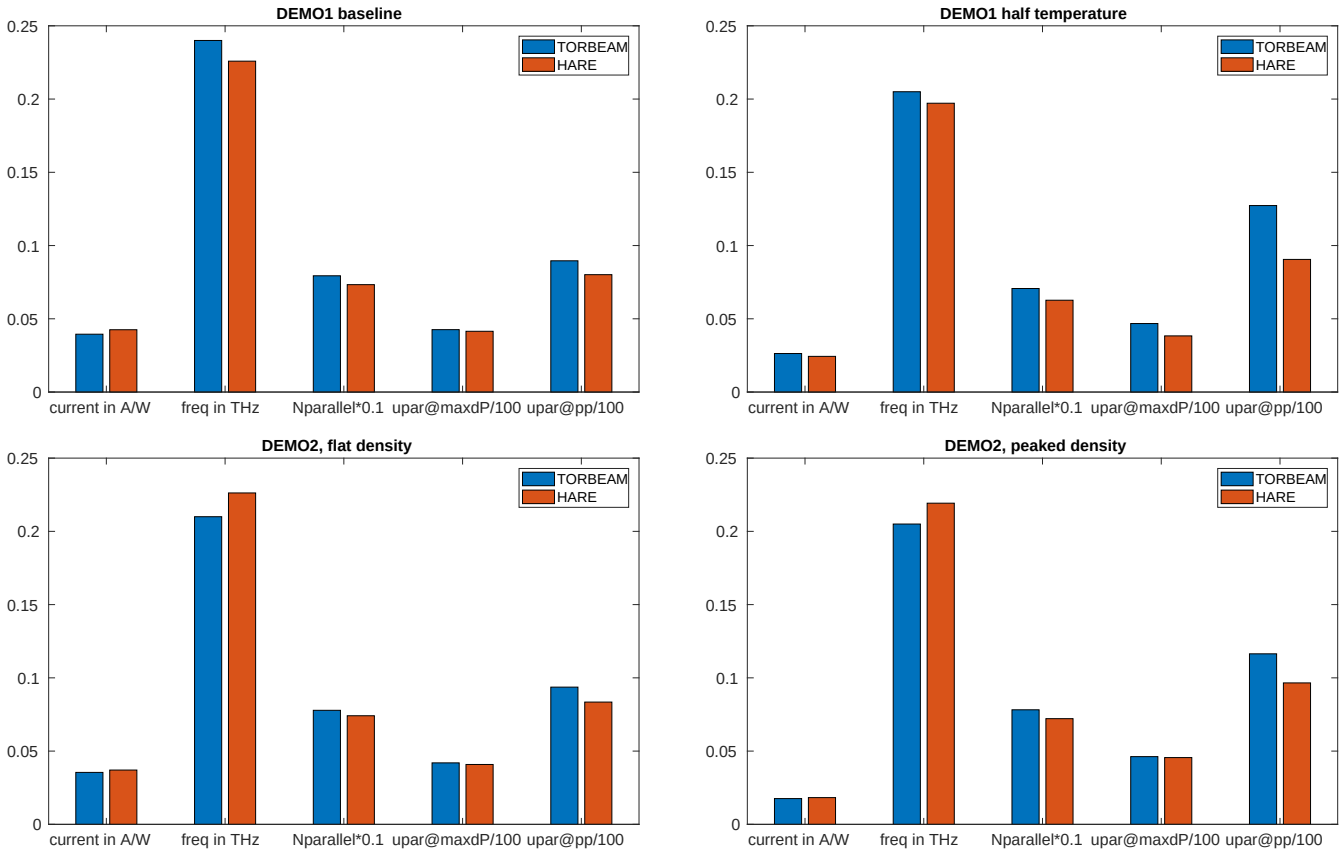

Figure 7: *Comparison between* `HARE` *results and full* `TORBEAM` *optimization for driven current, optimum beam frequency, parallel refractive index, $u_{\parallel -}$ at position of maximum absorption and $u_{\parallel -}$ at pinch point. The global parameters of the corresponding scenarios are reported in Table 1.*

where the numerical constant follows from expressing the various quantities in the units shown as a subscript (the density is in units of 10^{20} m^{-3}). A similar formula is also available in `PROCESS` [4].

In Table 2 a large variation of ζ_{CD} (of the order of $\pm 30\%$) can be observed across the scenarios discussed in this paper. Introducing a simple correction in the form $\tilde{\zeta}_{CD} = \zeta_{CD}(5 + Z_{\text{eff}})$, in order to incorporate the Z_{eff}-scaling predicted by Eq. (11), reduces somewhat the relative variation, which remains however large as compared to the (more physics-based) estimates of the `HARE` module. Moreover, Eq. (35) does not include in any form the saturation of the ECCD current at high temperature discussed in Sec. 4.4.

4.6 Radial variation

In the previous sections it was discussed how to obtain a fast but reliable estimate of the maximum driven current achievable through ECCD for given reactor parameters. Apart from high-temperature scenarios, where T_e exceeds 30 keV in a large portion of the plasma column, the maximum value of I_{CD} is achieved close to the plasma centre, $\rho \lesssim 0.2$. It is to be expected that I_{CD} drops with radius, due to the fact that the temperature decreases with ρ faster than the density. For consistent predictions, a systems code needs to know, if not a detailed driven-current profile, at least an estimate of the average current which can be driven across the plasma radius.

Fig. 9 presents a comparison of the current driven at different radial positions for two scenarios (DEMO1 and DEMO2-nflat), as obtained through different methods. The black

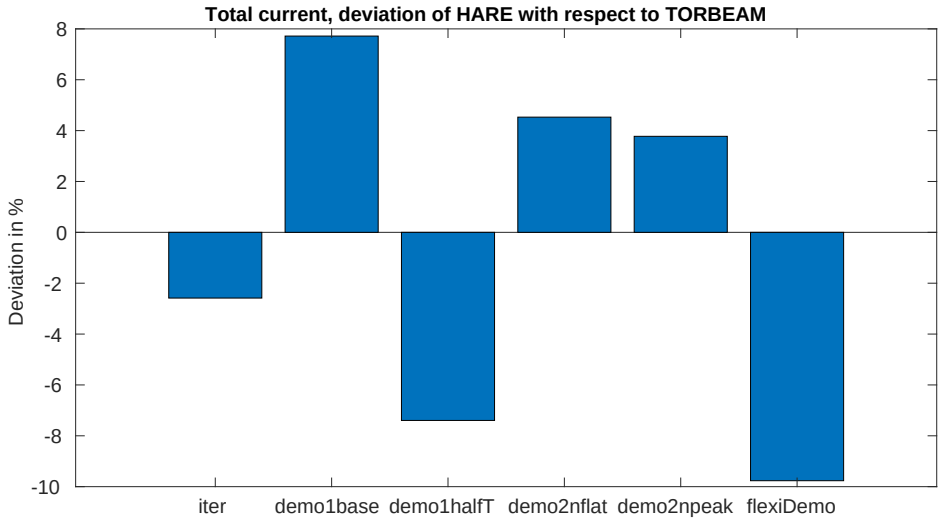

Figure 8: *Deviation of the* `HARE` *prediction for the total driven current with respect to the full* `TORBEAM` *optimization.*

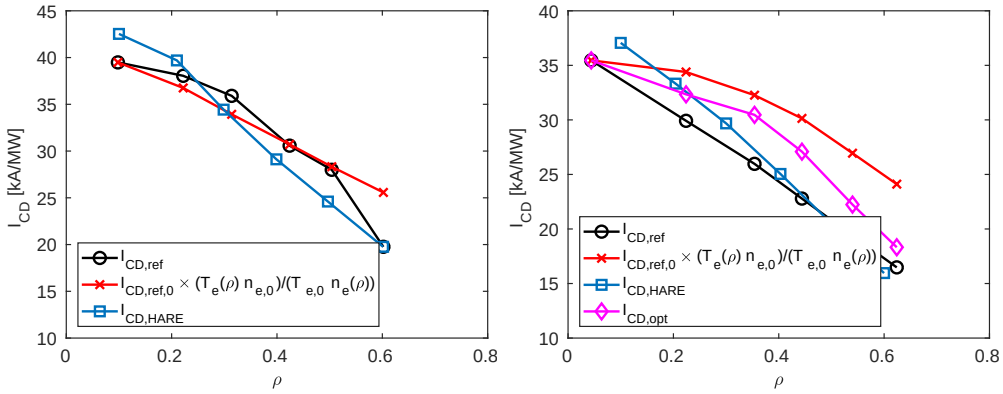

Figure 9: *Radial variation of the driven EC current* I_{CD} *as obtained by (a) varying the injection angles keeping the optimum antenna position and frequency fixed (*$I_{CD,ref}$*, black circles); (b) rescaling of the maximum value* $I_{CD,0}$ *with the local temperature-to-density ratio (red crosses); (c) from the* `HARE` *module (blue squares), for DEMO1 (left) and DEMO2-nflat (right) parameters. Also shown in the right panel is the profile obtained by varying also frequency and launch position to obtain higher* I_{CD} *values (magenta diamonds).*

	$\zeta_{CD}/\zeta_{CD,DEMO1}$	$\tilde{\zeta}_{CD}/\tilde{\zeta}_{CD,DEMO1}$
ITER	1.22	1.18
DEMO1	1.00	1.00
DEMO1-half T_e	1.33	1.33
DEMO2 nflat	0.72	0.94
DEMO2 npeak	0.86	1.12
flexi-DEMO	1.13	0.99

Table 2: *Values of ζ_{CD} and $\tilde{\zeta}_{CD} = \zeta_{CD} \times (5 + Z_{eff})$, divided by the respective values found for DEMO1 parameters ($\zeta_{CD} = 0.38$, $\tilde{\zeta}_{CD} = 2.7$), for the different scenarios discussed in the paper. A large variation, in particular of ζ_{CD}, can be observed.*

circles show the `TORBEAM` results obtained by keeping frequency and launch position as in the best (central) case and varying the launch angles (α, β) following the path of maximum current as a function of ρ suggested by the contour levels of the current optimization, as shown e.g. in Fig. 2 (left), for the two scenarios considered here. The red crosses show the results of a simple rescaling of the peak current value of the driven current $I_{CD,0}$ with the local density and temperature. The blue squares correspond to the `HARE` predictions taking the values of n_e and T_e at the selected radial location. It can be seen that the three methods lead to similar estimates. In the DEMO2-nflat scenario (Fig. 9, right panel), a further `TORBEAM` profile (magenta diamonds), showing an "optimized" scenario obtained by varying also antenna position and frequency to increase the driven current, is added in order to estimate the range of variability of the "reference" solution. Based on these results, it is concluded that a reasonable estimate of the radial variation of the EC driven current can be obtained by calculating the optimum (central) driven current $I_{CD,0}$ and rescaling it as

$$I_{CD}(\rho) = I_{CD,0} \frac{T_e(\rho) n_e(0)}{T_e(0) n_e(\rho)}. \tag{36}$$

For core temperatures $\gtrsim 60$ keV, the central region of the plasma might exhibit a depletion of the achievable ECCD efficiency due to the strong absorption at outer radii. These temperatures, however, are far from optimum both because of the departure of the fusion cross section from a quadratic scaling and the high level of radiation (mostly synchrotron) predicted at these temperatures [27].

As it is in general the case for reactor configurations emerging from systems-code optimizations, which need to be verified through more comprehensive scenario development employing e.g. 1.5-dimensional transport simulations, also the best-ECCD scenarios predicted through simplified approaches, like that employed in `HARE`, need to be checked through explicit ray/beam tracing calculations once the corresponding magnetic equilibria and kinetic profiles have been determined.

5 Discussion and conclusions

In this paper, the basic features of ECCD as described by the adjoint method for linear wave-particle interaction have been analyzed in order to infer under which conditions optimum current drive can be expected. The goal was the development of a fast but accurate estimate of the ECCD efficiency to be employed, for example, in systems codes where the calculation of the current driven by auxiliary heating systems is but a small part of the code operation. The approach followed here is to carry out the evaluation of ECCD efficiency numerically (judged as a feasible burden for the targeted applications) instead of looking for ways to simplify the response function. The latter is still a feasible option which could be explored if needed. A single evaluation of the ECCD efficiency is

performed employing parameters that should correspond to "optimum" ECCD conditions. The main physics assumption of the present model is that optimum ECCD conditions correspond to the maximum energy of the resonant electrons which can be reached being still consistent with the requirement of sufficient absorption. This implies that the energy of the resonant electrons can be increased with the temperature by increasing both the injected frequency and the parallel wave vector. To avoid the problem of harmonic overlap (parasitic absorption by the next harmonic with poor current drive), the increase of ω and $N_{\|}$ with the temperature is capped at 30 keV. For typical parameters envisaged in a tokamak reactor, the frequency for optimum current drive is found to be approximately by a factor 1.4 higher than the cyclotron frequency computed at nominal magnetic field on axis, in agreement with previous studies [25, 3] and the present results.

As presented here, the proposed method focuses on ECCD scenarios employing ordinary-mode heating at the fundamental cyclotron resonance, which is the scheme of choice given the high values of B envisaged in a reactor and the technological difficulties related to the development of high-power gyrotrons in the frequency range above 200 GHz. Although an extension of the method to different ECCD schemes (e.g. $n = 2$ X-mode) has not been explored yet, no difficulty in principle is expected.

These ideas have been implemented in a new module called `HARE`, which determines, starting from global reactor parameters, the input values to be supplied to the current drive routine developed by Lin-Liu [12], modified such as to take into account momentum conservation in electron-electron collisions. For the scenarios analyzed in this paper, the deviation of the `HARE` predictions for the driven current with respect to the reference solutions obtained from an extensive scan of the input parameters (antenna position, frequency, launch angles) is below 10%. The computational effort for a run of `HARE` is below 0.1 ms. An optimization loop with `TORBEAM` usually needs several thousands of runs, each requiring a couple of seconds, i.e. an effort which is seven orders of magnitude higher. It should be stressed that even if the numerical burden were manageable, a systems code does not usually provide the input required by ray/beam tracing codes like `TORBEAM`.

It has been shown that the dependence of the total driven current on the radial position can be calculated by different calls of the `HARE` module for different values of ρ (and correspondingly of n_e and T_e), or simply by rescaling the central value of I_{CD} according to the ratio T_e/n_e. This approach might become inaccurate at very high temperatures (above $50 - 60$ keV), where the off-axis absorption reduces the power available for central ECCD. An estimate of this effect would require a fast and efficient evaluation of the first and second-harmonic absorption coefficients. This extension is left for future work. It is remarked that such high temperatures are unlikely to represent an attractive scenario for a tokamak fusion reactor due to the expected strong radiation losses (which increase with temperature faster than the fusion power) [27].

Acknowledgments

The authors would like to thank E. Fable for providing the DEMO scenarios employed in this study and N. Bertelli for useful discussions on higher-harmonic absorption.

References

[1] R. Wenninger, F. Arbeiter, J. Aubert, L. Aho-Mantila, R. Albanese, R. Ambrosino, C. Angioni, J.-F. Artaud, M. Bernert, E. Fable, *et al. Nuclear Fusion*, vol. 55, p. 063003, 2015.

[2] H. Zohm, C. Angioni, E. Fable, G. Federici, G. Gantenbein, T. Hartmann, K. Lackner, E. Poli, L. Porte, O. Sauter, G. Tardini, D. Ward, and M. Wischmeier *Nuclear Fusion*, vol. 53, p. 073019, 2013.

[3] E. Poli, G. Tardini, H. Zohm, E. Fable, D. Farina, L. Figini, N. B. Marushchenko, and L. Porte *Nuclear Fusion*, vol. 53, p. 013011, 2013.

[4] M. Kovari, R. Kemp, H. Lux, P. Knight, J. Morris, and D. J. Ward *Fusion Engineering and Design*, vol. 89, p. 3054, 2014.

[5] M. Kovari, F. Fox, C. Harrington, R. Kembleton, P. Knight, H. Lux, and J. Morris *Fusion Engineering and Design*, vol. 104, p. 9, 2016.

[6] R. Prater, D. Farina, Y. Gribov, R. W. Harvey, A. K. Ram, Y.-R. Lin-Liu, E. Poli, A. P. Smirnov, F. Volpe, E. Westerhof, and A. Zvonkov *Nuclear Fusion*, vol. 48, p. 035006, 2008.

[7] E. Poli, A. Bock, M. Lochbrunner, O. Maj, M. Reich, A. Snicker, A. Stegmeir, F. Volpe, N. Bertelli, R. Bilato, *et al. Computer Physics Communications*, vol. 225, p. 36, 2018.

[8] E. Poli, A. G. Peeters, and G. V. Pereverzev *Computer Physics Communications*, vol. 136, p. 90, 2001.

[9] T. M. Antonsen and K. R. Chu *Physics of Fluids*, vol. 25, p. 1295, 1982.

[10] R. W. Harvey and M. G. McCoy, *The CQL3D Fokker-Plank code*. GA Report GA-A20978, 1992.

[11] M. Brambilla, *Kinetic Theory of Plasma Waves*. Oxford: Clarendon Press, 1998.

[12] Y. R. Lin-Liu, V. S. Chan, and R. Prater *Physics of Plasmas*, vol. 10, p. 4064, 2003.

[13] N. B. Marushchenko, H. Maassberg, and Y. Turkin *Nuclear Fusion*, vol. 48, p. 054002, 2008.

[14] N. B. Marushchenko, H. Maassberg, and Y. Turkin *Nuclear Fusion*, vol. 49, p. 129801, 2009.

[15] R. H. Cohen *Physics of Fluids*, vol. 30, p. 2442, 1987.

[16] E. Westerhof *Transactions of Fusion Science and Technology*, vol. 49, p. 87, 2006.

[17] N. J. Fisch and A. H. Boozer *Physical Review Letters*, vol. 45, p. 720, 1980.

[18] D. Farina *Fusion Science and Technology*, vol. 52, p. 154, 2007.

[19] D. Farina *Fusion Science and Technology*, vol. 53, p. 130, 2008.

[20] E. Fable, C. Angioni, M. Siccinio, and H. Zohm *Fusion Engineering and Design*, vol. 130, p. 131, 2018.

[21] K. V. Ellis, H. Lux, E. Fable, R. Kembleton, and M. Siccinio *45th EPS Conference on Plasma Physics*, p. P2.1076, 2018.

[22] G. R. Smith, R. H. Cohen, and T. K. Mau *Physics of Fluids*, vol. 30, p. 3633, 1987.

[23] M. Bornatici, R. Cano, O. De Barbieri, and F. Engelmann *Nuclear Fusion*, vol. 23, p. 1159, 1983.

[24] V. Parail, R. Albanese, R. Ambrosino, J.-F. Artaud, K. Besseghir, M. Cavinato, G. Corrigan, J. Garcia, L. Garzotti, Y. Gribov, *et al. Nuclear Fusion*, vol. 53, p. 113002, 2013.

[25] R. W. Harvey, W. M. Nevins, G. R. Smith, B. Lloyd, M. R. O'Brien, and C. D. Warrick *Nuclear Fusion*, vol. 37, p. 69, 1997.

[26] T. C. Luce, Y.-R. Lin-Liu, R. W. Harvey, G. Giruzzi, P. A. Politzer, B. W. Rice, J. M. Lohr, C. C. Petty, and R. Prater *Physical Review Letters*, vol. 83, p. 4550, 1999.

[27] M. Siccinio, E. Fable, A. Angioni, S. Saarelma, A. Scarabosio, and H. Zohm *Nuclear Fusion*, vol. 58, p. 016032, 2018.